Identification of Bolted Joint Properties through Substructure Decoupling

Jacopo Brunetti[*], **Walter D'Ambrogio**[*], **Matteo Di Manno**[**], **Annalisa Fregolent**[**], **Francesco Latini**[**]

[*] Dipartimento di Ingegneria Industriale e dell'Informazione e di Economia, UniversitÃ dell'Aquila
Via G. Gronchi, 18 - I-67100, L'Aquila (AQ), Italy,
email: jacopo.brunetti@univaq.it, email: walter.dambrogio@univaq.it

[**] Dipartimento di Ingegneria Meccanica e Aerospaziale, UniversitÃ di Roma La Sapienza
Via Eudossiana 18, I 00184 Rome, Italy,
email: annalisa.fregolent@uniroma1.it, email: francesco.latini@uniroma1.it
email: matteo.dimanno@uniroma1.it

ABSTRACT

Substructure decoupling techniques, defined in the frame of Frequency Based Substructuring, allow to identify the dynamic behaviour of a structural subsystem starting from the known dynamics of the coupled system and from information about the remaining components. The problem of joint identification can be approached in the substructuring framework by decoupling jointed substructures from the assembled system. In this case, information at the coupling DoFs of the assembled structure are necessary and this could be a problem if the interface is inaccessible for measurements. Expansion techniques can be used to obtain the dynamics on inaccessible (interface) DoFs starting from accessible (internal) DoFs. A promising technique is the System Equivalent Model Mixing (SEMM) that combines numerical and experimental models of the same component to obtain a hybrid model. This technique has been already used in an iterative coupling-decoupling procedure to identify the linear dynamic behaviour of a joint, with a Virtual Point description of the interface. In this work, a similar identification procedure is applied to the Brake Reus Beam benchmark to identify the linear dynamic behaviour of a three bolted connection at low levels of excitation. The joint is considered as a third independent substructure that accounts for the mass and stiffness properties of the three bolts, thus avoiding singularity in the decoupling process. Instead of using the Virtual Point Transformation, the interface is modelled by performing a modal condensation on remote points allowing deformation of the connecting surfaces between subcomponents. The purpose of the study is to highlight numerical and ill-conditioning problems that may arise in this kind of identification.

Keywords: Experimental Substructuring, Decoupling, Joint Identification, Model Mixing, Deformable Connecting Surfaces.

1 INTRODUCTION

Most of the engineering structures are composed of different parts connected together using bolted joints, tape and fir-tree joints. These joints can modify locally the mass, stiffness and damping properties of the assembled structure [1]. For this reason, it is useful to identify the characteristics of the joint in order to understand its effects

on the dynamics of the whole system. This could allow to use the identified joint in other analyses to evaluate the dynamics of assemblies that present the same type of connection. Substructuring techniques are useful for both the identification and for the use of the identified joint in other configurations. A general framework on dynamic substructuring is provided by De Klerk et al. in [2], where the approaches in physical, modal and frequency domain are presented supposing that the systems can be described by linear models. Substructuring techniques are broadly used because, among other advantages, they allow to combine experimental and numerical models [3, 4]. Dealing with experimental data, the substructuring approach in frequency domain, called Frequency Based Substructuring (FBS) [5] is the most advantageous. The substructuring approach allows to solve both the direct and the inverse problem, i.e. coupling and decoupling, respectively. The substructure coupling [6] consists in the identification of the dynamic behaviour of an assembled system starting from the known dynamic behaviour of the component subsystems. The DoFs of the assembled system can be partitioned into internal DoFs (not belonging to the couplings) and coupling DoFs. Inversely, substructure decoupling [7, 8, 9, 10, 11] consists in the identification of an unknown component subsystem from the known dynamic behaviour of the assembled system and of the residual part of the assembly.

Substructure decoupling can be used to perform the identification of the characteristics of a joint considered as a subsystem connected to the other physical subsystems of the assembly [12, 13, 14] In order to obtain the dynamic behaviour of the joint substructure at coupling DoFs, substructure decoupling requires the information of the assembled structure at least, on the coupling DoFs. This could be a problem if the joint interface is not accessible for measurements, but it can be overcome by using for example System Equivalent Model Mixing (SEMM) [4]. It performs coupling and decoupling operations between the numerical and the experimental model of the same component to obtain a hybrid model in which the experimental dynamics measured at accessible DoFs is expanded on inaccessible DoFs. In [15], the inaccessible dove-tail joint of a bladed disk structure is analyzed and the SEMM technique is implemented as an iterative procedure [16] to identify the properties of the connection. In that application, even if there is not a physical joint, the connection itself is considered as a third independent substructure and the dynamics at the connecting DoFs is obtained by using the Virtual Point Transformation (VPT) [17].

In this work, a modification to the joint identification procedure described previously is presented. The SEMM models of each substructure and of the coupled assembly are derived as usual. Nevertheless, the following modifications are introduced with reference to a bolted joint. First, in the iterative procedure, the initial guess for the joint is modeled as a lumped parameter system composed of two masses connected through elastic elements. In particular, the mass property is not fictitious but it is derived from the mass of the bolts in the real junction. Secondly, in order to account for the deformation of the connection interface, remote points are used to represent its dynamics instead of using the virtual points. This is done to deal with interface regions that are of finite length with respect to the assembled structure and can not be considered as rigid. The devised procedure is applied to identify the properties of the bolted joint of a numerically simulated Brake-Reuss Beam. This kind of structure was designed and used by Brake [1] to study friction in bolted joints and it is composed of two identical beams with square cross-section that are jointed together through three bolts at their common end. The purpose of the study is to highlight numerical and ill-conditioning problems that may arise in this kind of identification.

2 THEORETICAL BACKGROUND

In this section, the methods used to obtain the Frequency Response Functions (FRFs) of the models are described. In particular, the theory of LM-FBS and the SEMM method are presented.

2.1 Coupling using LM-FBS

Considering a number n of uncoupled substructures, the equation of motion that describes the r-th substructure in the frequency domain, can be written as:

$$\{u(\omega)\}^{(r)} = [Y(\omega)]^{(r)} \left(\{f(\omega)\}^{(r)} + \{g(\omega)\}^{(r)}\right) \tag{1}$$

where $\{u(\omega)\}^{(r)}$ is the response vector, $\{f(\omega)\}^{(r)}$ is the external force vector, $\{g(\omega)\}^{(r)}$ is the vector of connecting forces with other subsystems and $[Y(\omega)]^{(r)}$ is the FRF.
The equations of motion of the n subsystems to be coupled can be written in diagonal form as:

$$\{u\} = [Y]\left(\{f\} + \{g\}\right) \tag{2}$$

with

$$[Y] = \begin{bmatrix} [Y]^{(1)} & & \\ & \ddots & \\ & & [Y]^{(n)} \end{bmatrix}, \quad \{u\} = \begin{Bmatrix} \{u\}^{(1)} \\ \vdots \\ \{u\}^{(n)} \end{Bmatrix}, \quad \{f\} = \begin{Bmatrix} \{f\}^{(1)} \\ \vdots \\ \{f\}^{(n)} \end{Bmatrix}, \quad \{g\} = \begin{Bmatrix} \{g\}^{(1)} \\ \vdots \\ \{g\}^{(n)} \end{Bmatrix} \tag{3}$$

where the explicit frequency dependence is omitted.
Substructures can be coupled by imposing the compatibility and equilibrium conditions between the connecting DoFs. The compatibility condition at the connecting DoFs implies that any pair of matching DoFs $u_l^{(r)}$ and $u_m^{(s)}$ i.e. DoF l on subsystem r and DoF m on subsystem s have the same displacement, that is $u_l^{(r)} - u_m^{(s)} = 0$. This condition can be generally expressed by introducing the signed boolean matrix $[B]$:

$$[B]\{u\} = \{0\} \tag{4}$$

The equilibrium condition states that for the same pairs of connecting DoFs, the interface forces must be equal and opposite in sign, i.e. $g_l^{(r)} + g_m^{(s)} = 0$. In LM-FBS formulation, a set of unknown Lagrange multiplies $\{\lambda\}$ is introduced such that the equilibrium conditions can be rewritten using again the boolean matrix $[B]$:

$$[B]^T\{\lambda\} = -\{g\} \tag{5}$$

By substituting the interface forces $\{g\}$ into Eq. (5), the following system of equations is obtained:

$$\begin{cases} \{u\} = [Y]\left(\{f\} - [B]^T\{\lambda\}\right) \\ [B]\{u\} = \{0\} \end{cases} \tag{6}$$

It is possible to eliminate $\{\lambda\}$ and obtain the single line equation of LM-FBS:

$$\{u\} = \left[\bar{Y}\right]\{f\} \tag{7}$$

in which $[\bar{Y}]$ is the dually-assembled frequency response function for the system:

$$\left[\bar{Y}\right] = [Y] - [Y][B]^T\left([B][Y][B]^T\right)^{-1}[B][Y] \tag{8}$$

2.2 Decoupling using LM-FBS

Substructure decoupling allows to obtain the dynamic behaviour of an unknown subsystem A starting from the known behaviour of the assembled system AB and from information about the remaining component B, also referred as residual substructure. This procedure can be useful, for example, if substructure A is not accessible for direct measurements. In LM-FBS formulation, the decoupling process can be implemented by adding to the assembled system AB a fictitious substructure with an FRF opposite in sign to that of the residual subsystem B. This can be achieved by setting the following decoupled FRF matrix in Eq. (8):

$$[Y] = \begin{bmatrix} [Y]^{AB} & \\ & -[Y]^{B} \end{bmatrix} \tag{9}$$

When dealing with coupling operations, the compatibility and equilibrium conditions must be imposed on the coupling (or connecting) DoFs that are shared between substructures. This requires that both responses and forces must be determined on each coupling DoF thus resulting in square interface matrices $[B][Y][B]^T$.
Nevertheless, in decoupling operations the known structure AB and substructure B share both coupling and internal

DoFs, thus equilibrium and compatibility conditions can be imposed on internal and connecting DoFs resulting in an overdetermined problem in which the interface is addressed as extended. Furthermore, compatibility and equilibrium can be specified on different DoFs, thus resulting in distinct boolean matrices $[B_C]$ and $[B_E]$ for displacement and equilibrium. For this reason, Eq. (8) needs to be adapted by defining the coupled FRF matrix $[\bar{Y}]$ in which the pseudo-inverse operator $(\bullet)^+$ is used for the inversion of the interface matrix $[B_C][Y][B_E]^T$.

$$\left[\bar{Y}\right] = [Y] - [Y]\,[B_E]^T\,([B_C]\,[Y]\,[B_E]^T)^+\,[B_C]\,[Y] \tag{10}$$

2.3 System Equivalent Model Mixing

The SEMM is a technique based on the LM-FBS formulation that expands the information measured on some DoFs of the experimental model on some DoFs of the numerical one by performing coupling and decoupling operations. In this way, the considered component is described by a hybrid model in which it is possible to have information on inaccessible DoFs by exploiting measured data of the experimental model. In order to briefly explain how this method is derived, the DoFs of the component can be classified in different sets [15]:

- $\{u_c\}$: compatibility DoFs where response is measured;
- $\{u_e\}$: equilibrium DoFs where impacts are applied;
- $\{u_o\}$: other DoFs that are measured but are only used for validation purposes;
- $\{u_b\}$: boundary (or coupling) DoFs that are assumed to be inaccessible for measurements and excitation.

The different models involved in the expansion process are described below:

- *Parent model* $[Y]^{par}$: numerical model defined on the global set of DoFs $\{u_g\}$:

$$[Y]^{par} = \begin{bmatrix} [Y_{cc}] & [Y_{ce}] & [Y_{co}] & [Y_{cb}] \\ [Y_{ec}] & [Y_{ee}] & [Y_{eo}] & [Y_{eb}] \\ [Y_{oc}] & [Y_{oe}] & [Y_{oo}] & [Y_{ob}] \\ [Y_{bc}] & [Y_{be}] & [Y_{bo}] & [Y_{bb}] \end{bmatrix}^{par} \qquad \text{and} \qquad \{u_g\} = \begin{Bmatrix} \{u_c\} \\ \{u_e\} \\ \{u_o\} \\ \{u_b\} \end{Bmatrix} \tag{11}$$

- *overlay model* $[Y]^{ov}$: experimental model of the component obtained by measuring on the compatibility DoFs $\{u_c\}$ when exciting at the equilibrium DoFs $\{u_e\}$.

$$[Y]^{ov} = [Y_{ce}]^{ov} \tag{12}$$

- *removed model* $[Y]^{rem}$: it is a numerical condensed form of the parent model used to remove the parent dynamics from the component. In the so called "Extended SEMM" presented in [4], the removed model is defined on the global set of DoFs and coincides with the parent model:

$$[Y]^{rem} = [Y_{gg}]^{par} \tag{13}$$

- *hybrid model* $[Y]^{SEMM}$: result of SEMM expansion. It is defined on the same DoFs of the parent model. For the Extended SEMM equation, specified for the global set of DoFs $\{u_g\}$, it is [15]:

$$\left[\overline{Y}\right]^{SEMM} = [Y_{gg}]^{par} - [Y_{gg}]^{par}\,([Y_{cg}]^{par})^{+}([Y_{ce}]^{par} - [Y_{ce}]^{ov})([Y_{ge}]^{par})^{+}\,[Y_{gg}]^{par} \tag{14}$$

The expansion technique is described in Figure 1.

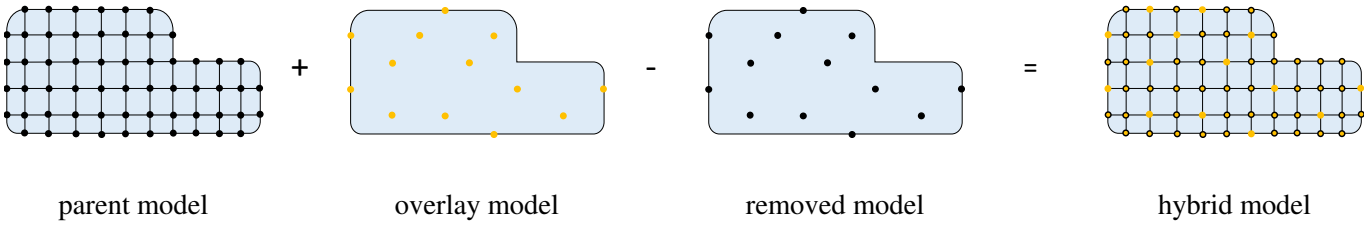

Figure 1: SEMM expansion technique. The dynamics measured on the DoFs of the experimental Overlay model, are overlapped in the numerical model that provide the DoF set of the component. The dynamics of the numerical model are then subtracted by decoupling the Removed model.

3 JOINT IDENTIFICATION PROCEDURE

In this section, the identification procedure of the joint connecting substructure A and substructure B is described considering that the connecting interface is not accessible for measurements. The joint is considered as a third independent substructure J with given mass and stiffness properties. Thus, its behaviour can be obtained by decoupling the dynamics of substructures A and B from the dynamic behaviour of the assembled structure AB as shown in Figure 2. As seen from Figure 2, substructures A and B have both internal and boundary DoFs, and the

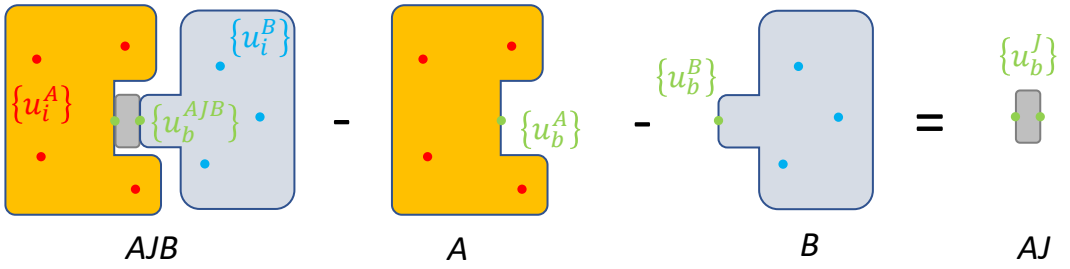

Figure 2: Joint identification through substructure decoupling. The internal DoFs are indicated as $\{u_i\}$; $\{u_b\}$ are the boundary DoFs.

joint J is defined over the same boundary DoFs of A and B, that are not known if the interface is not accessible for measurements. Thus, in order to identify the joint, the dynamic behaviour of the assembled structure must be known at the boundary DoFs $\{u_b\}^A$ and $\{u_b\}^B$. For this reason, it is necessary to obtain the SEMM models either of the assembled structure and also of the decoupled substructures A and B. The FRF of the joint at iteration i $[Y]_i^J$ is used together with the SEMM models of substructures A and B to obtain the decoupled FRF matrix $[Y]_{i+1}$:

$$[Y]_{i+1} = \begin{bmatrix} [Y]^{A,SEMM} & & \\ & [Y]_i^J & \\ & & [Y]^{B,SEMM} \end{bmatrix} \tag{15}$$

used in Eq. (8) to obtain the parent model of the assembled structure $[Y]_{i+1}^{AB,par}$ that contains the boundary DoFs but lacks of the real dynamics introduced by the joint. This information can be introduced in the model $[Y]_{i+1}^{AB,par}$ by performing a SEMM expansion using the experimental Overlay model $[Y]^{AB,ov}$ thus obtaining the Hybrid model $[Y]_{i+1}^{SEMM,par}$. The FRF of the joint substructure at iteration $i+1$ is then obtained by decoupling the SEMM models of substructures A and B from the assembly AB:

$$[Y]_{i+1}^J = \begin{bmatrix} [Y]_{i+1}^{AB,SEMM} & & \\ & -[Y]^{A,SEMM} & \\ & & -[Y]^{B,SEMM} \end{bmatrix} \tag{16}$$

Note that in order to start the procedure, an initial guess for the joint is estimated by assigning mass and stiffness matrices M_J and K_J and its FRF $[Y]_0^J$. The iterative algorithm stops when the following convergence criterion is satisfied:

$$\frac{\left|[Y_{ce}]_{i+1}^{AB,par} - [Y_{ce}]^{AB,ov}\right|_2}{\left|[Y_{ce}]^{AB,ov}\right|_2} < \varepsilon \tag{17}$$

4 BRAKE-REUSS BEAM MODEL

The joint identification procedure is applied to a Brake-Reuss Beam: it is composed of two identical beams with square cross-section that have half-height extension near one of their ends. The two beams can be overlapped in correspondence of the half-height extensions in order to be jointed with three bolts, thus forming a lap joint as shown in Figure 3. As seen from Figure 3, substructure A is clamped at one end both in the coupled and uncoupled

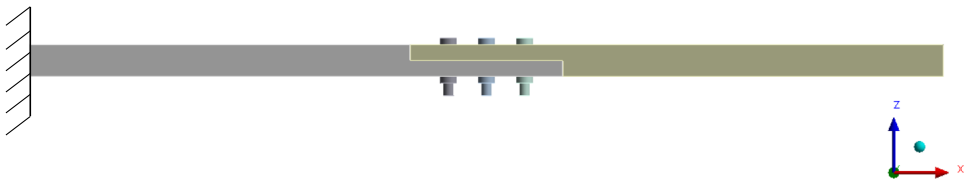

Figure 3: Brake Reuss Beam.

configuration, while substructure B is always unconstrained. The beams are made in steel alloy AISI-304 and the dimensions of the assembly are 720.9 x 25 x 25 mm. Each bolt consists of a screw M8x40 hexagon head and a M8 nut with washer under the bolt head and the nut. Both the beams and the assembly have been modeled in Ansys in order to build the parent and the overlay models to be used in the identification procedure outlined in Section 3. In the present work, the overlay model is obtained from numerical simulations instead of experimental tests in order to validate the identification procedure. Some important aspects need to be pointed out regarding the models of the beams and of the assembly.

4.1 SEMM models

A linear finite element model of each substructure is developed in Ansys. The interface surface of each beam is divided into five areas and the nodes belonging to each area are connected to a dependent remote point located in the middle of the area using Multi Point Constraint equations [18, 19] as shown in Figure 4. This assumption allows to retain the local flexibility of the interface.

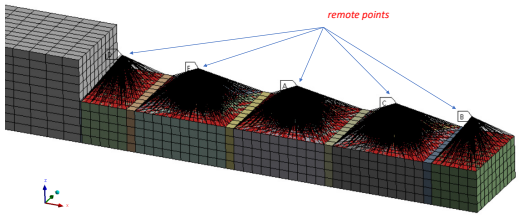

Figure 4: Remote points used to account for connecting surface deformation.

Since the SEMM model of each beam is needed, the following sets of DoFs are chosen:

$$\{u_g\}^A = \begin{Bmatrix} \{u_c\}^A \\ \{u_e\}^A \\ \{u_o\}^A \\ \{u_b\}^A \end{Bmatrix}, \quad \{u_g\}^B = \begin{Bmatrix} \{u_c\}^B \\ \{u_e\}^B \\ \{u_o\}^B \\ \{u_b\}^B \end{Bmatrix} \tag{18}$$

Note that the boundary DoFs $\{u_b\}^A$ and $\{u_b\}^B$ are located on the connecting surfaces and they are not accessible for measurement and excitation in the assembled configuration.
Regarding the SEMM model of the Brake Reuss Beam, in order to simulate the experimental Overlay Model of the assembled structure $[Y]^{AB,ov}$, a numerical FEM model is first generated (Figure 5). The remote points, previously

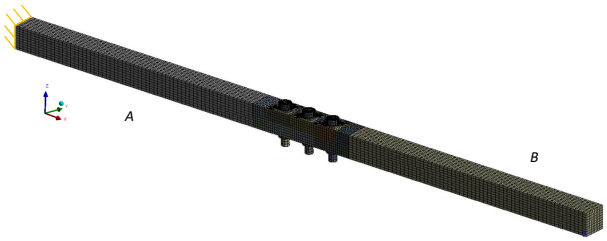

Figure 5: FE model of the Brake Reus Beam. Beam A is clamped at its end.

defined on the connecting surfaces of the beams, are deleted and the FE models of the three bolts are introduced. The built-in Bolt Pretension Tool of Ansys is used to apply an axial load to each bolt in order to simulate a tightening torque T of 14 Nm. The modes of the Brake Reuss Beam are computed with a nonlinear pre-stressed analysis that is able to account for bolt preload. The Mode Superposition Method implemented in [20] is used to numerically generate the overlay model of the assembled structure, that is defined on the same measurement DoFs $\{u_c\}^{AB}$ and excitation DoFs $\{u_e\}^{AB}$ of the two beams, i.e.:

$$\{u_c\}^{AB} = \begin{Bmatrix} \{u_c\}^A \\ \{u_c\}^B \end{Bmatrix} \qquad \{u_c\}^{AB} = \begin{Bmatrix} \{u_e\}^A \\ \{u_e\}^B \end{Bmatrix} \tag{19}$$

Regarding the parent model $[Y]^{AJB,par}$ shown in Section 3, it is generated as described in Figure 6 at each iteration: the SEMM models of the beams A and B are coupled with the joint substructure J by imposing compatibility and equilibrium conditions between the boundary DoFs of the two beams (translational and rotational DoFs of the blue dots) and the coupling DoFs of the joint (translational and rotational DoFs of the red dots). Thus, the DoFs of the parent model can be collected as follows:

$$\{u_g\}^{AB} = \begin{Bmatrix} \{u_g\}^A \\ \\ \{u_g\}^B \end{Bmatrix} \tag{20}$$

Note that, in Equation (20) the DoFs of the joint $\{u\}^J$ are not reported, as they are coincident with the boundary DoFs of the beams.
The joint is defined on 60 DoFs (both translational and rotational), that can be considered as 30 pairs of uncoupled 2-DoF systems composed by two masses connected through a spring element. The initial guess of the joint FRF $[Y]_o^J$ depends on five parameters: the mass m associated with each translational DoF, the translational stiffness k of the spring that connects two translational DoFs, the inertia I_r associated with each rotational DoFs and the rotational stiffness k_r that connects two pairs of rotational DoFs.

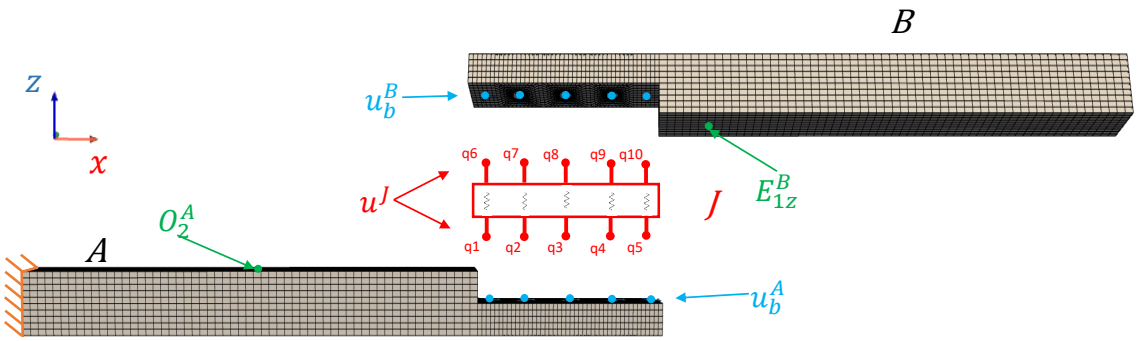

Figure 6: Generation of $[Y]^{AJB,par}$. The SEMM models of substructures A and B are coupled with the joint. The joint substructure is defined on the translational and rotational DoFs of the points $q1$-$q10$.

5 RESULTS

In this section, the results of the identification procedure applied to the Brake-Reuss Beam are discussed. It is necessary to point out that the results of the identification procedure depend either on the number and the position of measurement and excitation points considered in the generation of the overlay model and on the mass m used for the initial guess of the joint. These dependencies are discussed along with the results obtained in the case in which a sufficient number of experimental measurements and a good estimate of the mass value are used. Since the real behaviour of the joint is not known, the quality of the solution is evaluated by reconstructing the FRF of the parent model $[Y]^{AJB,par}$, obtained by coupling the SEMM models of beams A and B with the identified joint J, in one DoF not involved in the identification process, thus belonging to the set $\{u_o\}^{AB}$. The comparison between this parent model $[Y]^{AJB,par}$ with the FRF of the experimental model at the same DoF, provides meaningful information regarding the quality of the solution.

5.1 Effect of measurement points

The joint identification procedure used in this work is an inverse problem, thus the data space and the solution space, i.e. the dimensions of the overlay model and of the joint substructure respectively, must be carefully chosen. As seen in section 4.1, the joint substructure is defined on a set of 60 DoFs, thus resulting in a FRF matrix $[Y]^J$ with dimension (60×60). The overlay model $[Y]^{AB,ov}$ instead, is defined on N_c measurement DoFs $\{u\}^{AB}$ and on N_e excitation DoFs $\{u_e\}^{AB}$, thus resulting in a matrix with dimension $(N_c \times N_e)$. In this section, the dependence of the solution on the choice of measurement points is investigated. First, the dependence of the solution on the position of the measured DoFs is discussed. In Figure 7, the results of the identification procedure are shown for two different sets of measurement points S_1 and S_2. They have an equal number of measurement and excitation DoF ($N_c = N_e = 25$). In Figure 7(a), the joint FRF between the DoFs q_3z and q_8z, obtained for S_1 (blue line) and S_2 (orange line) are shown, while in Figure 7(b) the corresponding reconstructed FRFs at validation DoF O_2z ($O_2z \in \{u\}_o^A$) and the FRF of the experimental model are compared. Note that the validation DoF O_2z is part of the experimental model, but is kept out of the overlay model, i.e. it is not used in the identification procedure. It can be seen from Figure 7(a) that in the frequency band from 0 Hz to about 250 Hz, the two FRFs of the joint are quite in agreement and both are able to reconstruct the behaviour of the Brake Reuss Beam in Figure 7(b). From 250 Hz on, the FRFs of the joint present a relevant scattering and consequently the corresponding reconstructed FRFs cannot be considered as reliable. The difference in solutions obtained with two different sets of DoFs could be due to ill-conditioning. In particular, the problem could be underdetermined, i.e. the used measurements are not sufficient to reconstruct the real dynamics of the joint. As stated before, the joint FRF is defined on a set of 60 DoFs. Thus, by defining the overlay model on a number $Nc = 60$ of measurement DoFs and $N_e = 60$ of excitation DoFs, the problem is determined. The corresponding identified joint FRF is represented by the red curve in Figure 8 that presents a lower scattering with respect to the previous results. Also, the reconstruction of the behaviour of the Brake Reuss Beam (the FRF of the validation point O_2z) is in good agreement with the reference curve (dashed

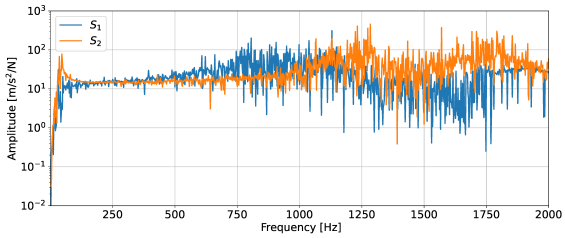

(a) Joint FRF between DoFs q_3z and q_8z.

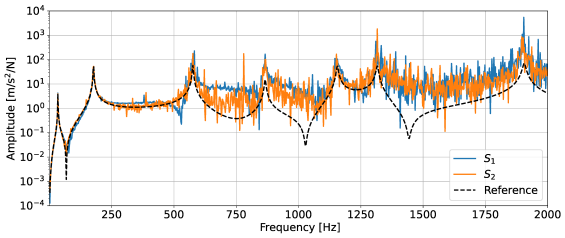

(b) FRF of the Brake Reuss Beam between the DoFs O_2z on beam A and E_1z on beam B.

Figure 7: Results with $N_c = N_e = 25$ and $N_e = 25$; the blue and orange curves refer to different sets of DoFs, S_1 and S_2 respectively; the black reference curve in (b) is obtained from the simulated experimental model.

black line) up to 1300 Hz. However, it could be possible that not all the DoFs of the joint substructure are necessary. To investigate this aspect, a lower number of measurement DoFs is considered. In Figure 8, the orange curve refers to $[Y]^{AB,ov}(34 \times 34)$ and the green curve refers to $[Y]^{AB,ov}(36 \times 36)$. In both cases, the reduction of the number of

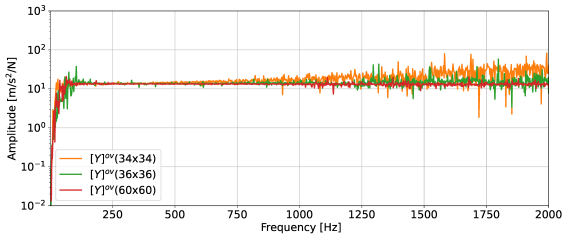

(a) Joint FRF between DoFs q_3z and q_8z.

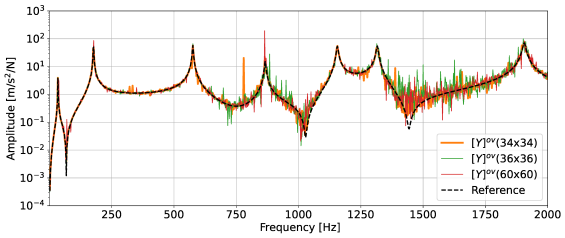

(b) FRF of $[Y]^{AJB,par}$ between DoFs O_2z on beam A and E_1z on beam B.

Figure 8: Solution of the identification problem with different dimension of $[Y]^{AB,ov}$: (34×34) (orange curve), (36×36) (green curve) and (60×60) (red curve); the reference curve in black is obtained from the simulated experimental model.

measured DoFs introduces scattering in the joint FRF (Figure 8(a)) that propagates in the reconstructed FRF of the assembled structure (Figure 8(b)). However, by comparing the results in Figure 7 and Figure 8, it can be noted that the solution improves as the number of measurement DoFs increases.

5.2 Effect of initial guess mass value

In order to start the joint identification procedure, an initial guess model of the connection is required. It is expected that the initial guess value does not affect the final solution and this is verified for the case in which the overlay model has dimension (60×60). However, when the dimension of the overlay model decreases the choice of the initial guess can affect the solution. Therefore, to evaluate the effect of different initial guess model on the solution, the mass value m is increased from 0.005 Kg to 0.04 Kg. In Figure 9, the results of the joint identification carried out with the overlay model $[Y]^{AB,ov}(34 \times 34)$ are shown for two choice of the initial guess mass: $m = 0.005$ Kg and $m = 0.04$ Kg. The two solutions are different, even if they are able to reconstruct the behaviour of the reference model. In particular, it can be noted that above 1500 Hz, where the scattering level becomes more relevant, the joint FRF tends to converge to the initial guess curve. Using an overlay model of dimension (36×36), the initial guess change does not affect the solution (Figure 10).

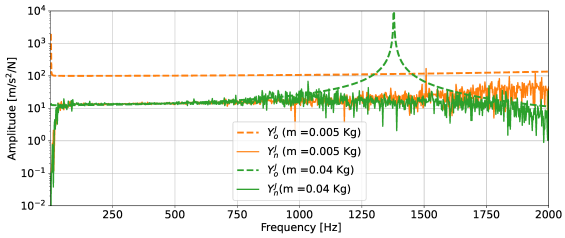

(a) Joint FRF between DoFs q_3z and q_8z.

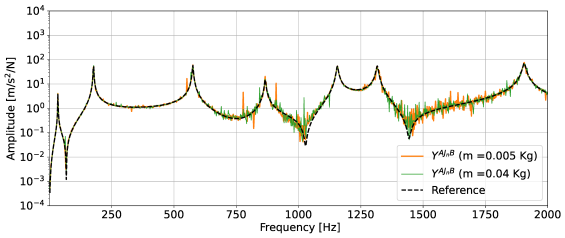

(b) FRF of $[Y]^{AJB,par}$ between the DoFs O_2z on beam A and E_1z on beam B.

Figure 9: Solution of the identification problem with $[Y]^{AB,ov}(34\times34)$, for different values of the initial guess mass m; initial guess FRFs (dashed line); identified FRFs (solid line); the reference curve in black is obtained from the simulated experimental model.

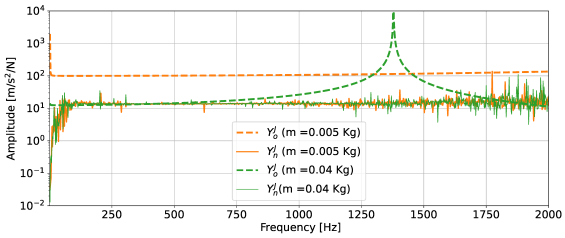

Figure 10: Joint FRF between DoFs q_3z and q_8z with $[Y]^{AB,ov}$(36x36), for different values of the initial guess mass m: initial guess FRFs (dashed line); identified FRFs (solid line).

5.3 Identified joint

The physical interpretation of the identified joint can be carried out by looking at its accelerance and receptance FRFs. The joint identified with the overlay model $[Y]^{AB,ov}(36\times36)$ is considered in the following. In Figure 11, the receptance FRF and the accelerance FRFs between the DoFs q_3z and q_8z are shown for the identified joint. These two points are located in correspondence of the central bolt of the Brake Reuss Beam. It can be seen from the

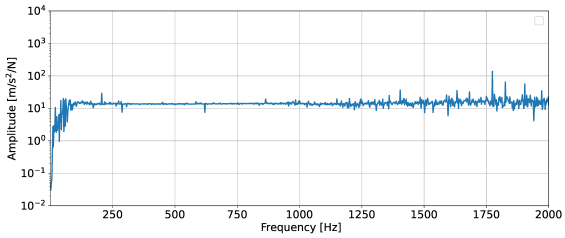

(a) Receptance FRF.

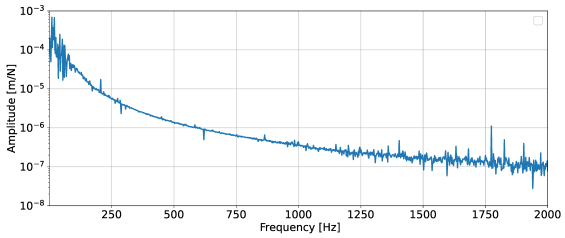

(b) Accelerance FRF.

Figure 11: FRFs of the identified joint between the DoFs q_3z and the q_8z.

receptance FRF, that the joint has an initial peak at very low frequency and this is due to the fact the the identified joint substructure is in free-free conditions, thus having rigid body modes. At high frequencies, the accelerance of the joint presents a typical mass line.

6 CONCLUSIONS

In this work, the problem of joint identification is approached by decoupling jointed substructures from the assembled system. In order to obtain information at the coupling DoFs, the System Equivalent Model Mixing expansion has been used and the interface is described using remote points thus taking into account the deformation of the connecting surfaces. The proposed approach has been applied to identify the bolted joint of a numerically simulated Brake Reuss Beam. The obtained results highlight that the choice of the number and location of the measurement DoFs affects the quality of the identification. In fact, by using a set of measurement that makes the problem determined, the quality of the joint identification is quite satisfactory. The set of measurement can be reduced providing acceptable result in a lower frequency band. Conversely, an excessive reduction of the number of measurement DoFs leads to numerical ill-conditioning of the problem due to the lack of relevant information to correctly identify the dynamic behaviour of the joint. Future developments aim at investigating the effect of measurement noise and at applying the identification procedure to different kind of joints using also experimental data.

ACKNOWLEDGEMENTS

This research is supported by University of Rome La Sapienza and University of L'Aquila.

REFERENCES

[1] **Brake, M. R. W.**, The Mechanics of Joined Structures, Springer International Publishing, 2018.

[2] **de Klerk, D., Rixen, D. J.** and **Voormeeren, S. N.**, *General Framework for Dynamic Substructuring: History, Review and Classification of Techniques*, AIAA Journal, Vol. 46, No. 5, pp. 1169–1181, 2008.

[3] **Brunetti, J., Culla, A., D'Ambrogio, W.** and **Fregolent, A.**, *Experimental dynamic substructuring of the Ampair wind turbine test bed*, Vol. 1, pp. 15–26, 2014.

[4] **Klaassen, S., van der Seijs, M.** and **de Klerk, D.**, *System equivalent model mxing*, Mechanical Systems and Signal Processing, Vol. 105, pp. 90–112, 2018.

[5] **Jetmundsen, B., Bielawa, R. L.** and **Flannelly, W. G.**, *Generalized Frequency Domain Substructure Synthesis*, Journal of The American Helicopter Society, Vol. 33, pp. 55–64, 1988.

[6] **de Klerk, D., Rixen, D. J.** and **de Jong, J.**, *The frequency based substructuring (FBS) method reformulated according to the dual domain decomposition method*, *Proceedings of the 24th International Modal Analysis Conference, A Conference on Structural Dynamics*, pp. 1–14, 2006.

[7] **D'Ambrogio, W.** and **Fregolent, A.**, *Direct decoupling of substructures using primal and dual formulation*, *Linking Models and Experiments*, Vol. 2 of *Conference Proceedings of the Society for Experimental Mechanics Series*, 2011.

[8] **D'Ambrogio, W.** and **Fregolent, A.**, *Decoupling procedures in the general framework of Frequency Based Substructuring*, 2009.

[9] **D'Ambrogio, W.** and **Fregolent, A.**, *The role of interface DoFs in decoupling of substructures based on the dual domain decomposition*, Mechanical Systems and Signal Processing, Vol. 24, No. 7, pp. 2035–2048, 2010.

[10] **Voormeeren, S.** and **Rixen, D.**, *A dual approach to substructure decoupling techniques*, *Structural Dynamics, Volume 3*, pp. 601–616, Springer, 2011.

[11] **Voormeeren, S. N.** and **Rixen, D. J.**, *A family of substructure decoupling techniques based on a dual assembly approach*, Mechanical Systems and Signal Processing, Vol. 27, pp. 379–396, 2012.

[12] **Haeussler, M., Klaassen, S.** and **Rixen, D.**, *Comparison of substructuring techniques for experimental identification of rubber isolators dynamic properties*, *ISMA 2018 International Conference on Noise and Vibration Engineering*, 2018.

[13] **Haeussler, M., Klaassen, S.** and **Rixen, D.**, *Experimental twelve degree of freedom rubber isolator models for use in substructuring assemblies*, Journal of Sound and Vibration, Vol. 474, pp. 115253, 2020.

[14] **Klaassen, S., E., C.** and **H.N., z.**, *Identifying the joint dynamics of a bolted beam system by using FRF decoupling and the SEMM expansion technique*, 07 2019.

[15] **Saeed, Z., Klaassen, S. W. B., Firrone, C. M., Berruti, T. M.** and **Rixen, D. J.**, *Experimental Joint Identification Using System Equivalent Model Mixing in a Bladed-Disk*, Journal of Vibration and Acoustics, pp. 1–29, 2020.

[16] **Klaassen, S. W.** and **Rixen, D. J.**, *Using SEMM to Identify the Joint Dynamics in Multiple Degrees of Freedom Without Measuring Interfaces*, *Dynamic Substructures*, Vol. 4 of *Conference Proceedings of the Society for Experimental Mechanics Series*, pp. 87–99, Springer, 2020.

[17] **Van der Seijs, M., van den Bosch, D., Rixen, D.** and **Klerk, D.**, *An improved methodology for the virtual point transformation of measured frequency response functions in dynamic substructuring*, pp. 4334–4347, 06 2013.

[18] **Ansys**, Mechanical APDL Element Reference, ANSYS Inc, Release 2021 R2.

[19] **Ansys**, Mechanical APDL Theory Reference, ANSYS Inc, Release 2021 R2.

[20] **Bregar, T., El Mahmoudi, A., Kodric, M., Cepon, G., Boltezar, M.** and **Rixen, D. J.**, *Introducing pyFBS: An Open-Source Python Package for Frequency Based Substructuring and Transfer Path Analysis*, pp. 81–89, 2022.